Symmetry crossover in layered MPS_3 complexes (M = Mn, Fe, Ni) via near-field infrared spectroscopy

S. N. Neal,[1] H. -S. Kim,[2] K. R. O'Neal,[1] A. V. Haglund,[3] K. A. Smith,[1] D. G. Mandrus,[3,4]
H. A. Bechtel,[5] G. L. Carr,[6] K. Haule,[7] David Vanderbilt,[7] and J. L. Musfeldt[1,8,*]

[1] *Department of Chemistry, University of Tennessee, Knoxville, Tennessee 37996, USA*
[2] *Department of Physics and Astronomy, Rutgers University, Piscataway, New Jersey 08854, USA*
[3] *Department of Materials Science and Engineering,*
University of Tennessee, Knoxville, Tennessee 37996, USA
[4] *Materials Science and Technology Division, Oak Ridge National Laboratory, Oak Ridge, Tennessee 37831, USA*
[5] *Advanced Light Source Division, Lawrence Berkeley National Laboratory, Berkeley, California 94720, USA*
[6] *National Synchrotron Light Source II, Brookhaven National Laboratory, Upton, New York 11973, USA*
[7] *Department of Physics and Astronomy, Rutgers University, Piscataway, New Jersey 08854, USA*
[8] *Department of Physics and Astronomy, University of Tennessee, Knoxville, Tennessee 37996, USA*

(Dated: May 4, 2020)

We employ synchrotron-based near-field infrared spectroscopy to reveal the vibrational properties of bulk, few-, and single-sheet members of the MPS_3 (M = Mn, Fe, Ni) family of materials and compare our findings with complementary lattice dynamics calculations. $MnPS_3$ and the Fe analog are similar in terms of their symmetry crossovers, from $C2/m$ to $P\bar{3}1m$, as the monolayer is approached. These states differ as to the presence of a C_3 rotation around the metal center. On the other hand, $NiPS_3$ does not show a symmetry crossover, and the lack of a B_u symmetry mode near 450 cm^{-1} suggests that C_3 rotational symmetry is already present - even in the bulk material. We discuss these findings in terms of local symmetry and temperature effects as well as the curious relationship between these symmetry transformations and those that take place under pressure.

Introduction

Complex chalcogenides like $CrSiTe_3$, CrI_3, and $CuInP_2S_6$, are superb platforms for revealing the interplay between charge, structure, and magnetism and unusual states of matter that develop under external stimuli.[1–4] These van der Waals solids can be exfoliated into few- and single-layer sheets that sport a number of unexpected properties including quantum confinement, magnetic excitations and size-induced magnetic states, and symmetry breaking.[5–13] The MPS_3 (M = Mn, Fe, Ni) family of materials attracted our attention in this regard. These compounds are well-suited to the development of structure-property relations, and the connection between few- and single layer properties and those accessible under external stimuli are highly underexplored.

The MPS_3 (M = Mn, Fe, Ni) materials exist in the monoclinic space group $C2/m$.[14–16] Substitution of the metal center systematically alters the sheet thickness and van der Waals gap [Fig. 1(a)] as well as various bond lengths and angles.[16,17] Spectroscopy is unlocking properties suitable for optoelectronics applications,[18] and external stimuli reveal layer sliding, superconductivity, piezochromism, and driven magnetic states - just to name a few.[2,19–24] The properties of these materials also evolve under exfoliation. Raman scattering, which measures the behavior of even-symmetry (*gerade*) modes, is regularly employed to study few- and single-sheet materials - determining the number of layers, symmetry-breaking, electron-phonon coupling, even uncovering the suppression of magnetic order at the monolayer in $NiPS_3$.[13,25,26] Infrared spectroscopy is also a superb probe of local symmetry, revealing the behavior of odd-symmetry (*ungerade*) vibrational modes. It is, however, nearly impossible to apply traditional infrared techniques to an exfoliated sample because (i) long wavelength far infrared light has large diffraction-limited focal points,[27,28] and (ii) large area thin films[29–32] are not currently available for every complex chalcogenide of interest. Near-field infrared nanospectroscopy offers an im-

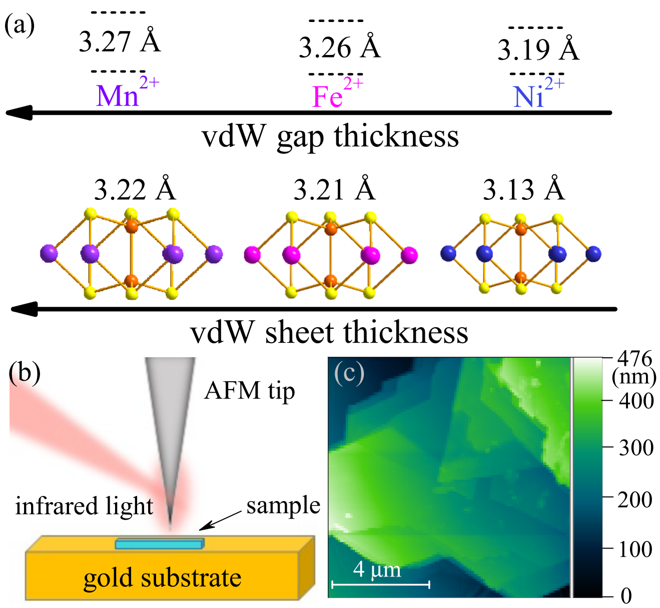

FIG. 1: (a) van der Waals gap size and sheet thickness as a function of metal-site substitution. (b) Schematic of an AFM cantilever tip directing light to the sample surface. (c) High resolution AFM image of few-layer $FePS_3$.

portant path forward. This technique fuses a high brightness, broadband light source, such as a synchrotron, with a Fourier transform infrared spectrometer and an atomic force microscope. In addition to imaging sheet topography, the tip focuses infrared light onto the sample with a 20×20 nm^2 spatial resolution [Fig. 1(b,c)] - sufficient for work on few- and single-layer sheets, domain walls, and plasmons.[33–35] Our team recently employed this technique to reveal a $C2/m \rightarrow P\bar{3}1m$ symmetry crossover in $MnPS_3$ as a function of sheet thickness.[34] Symmetry is higher in the monolayer due to a restoration of the three-fold rotation about the metal center. The availability of materials with different metal centers offers an opportunity to unravel structure-property relationships involving sheet thickness, symmetry, and local structure.

In order to explore symmetry effects in an important class of magnetic chalcogenides, we employed synchrotron-based near-field infrared spectroscopy to measure local lattice distortions in the MPS_3 (M = Mn, Fe, Ni) family of materials in bulk, few-, and single-layer form. Analysis of the odd-symmetry vibrational modes reveals that the B_u feature near 450 cm^{-1} is exceptionally sensitive to the presence (or absence) of the C_3 rotation about the metal center. Using this feature as a guide, we find that both $MnPS_3$ and the Fe analog display a $C2/m$ to $P\bar{3}1m$ transition with decreasing thickness whereas the third system, $NiPS_3$, retains its "C_3-ness". These findings are discussed in terms of the local structure, the stacking pattern, and temperature effects as well as slab thickness and van der Waals gap trends. Moreover, the space groups preferred by $MnPS_3$ at different sheet thicknesses are strikingly similar to those across the pressure-induced sliding and insulator-metal transitions,[23] suggesting that symmetry-driven properties in few- and single layer analogs can be accessed under pressure and strain as well.

Methods

Single crystals of $MnPS_3$, $FePS_3$, and $NiPS_3$ were grown using the chemical vapor transport process as described previously.[36] For near-field work, these crystals were mechanically exfoliated using thermal release tape and applied to the surface of a gold mirror. For far field studies, a pinhole was used to support crystals with appropriate optical density. Near-field infrared nano-spectroscopy was performed using Beamline 2.4 at the Advanced Light Source, Lawrence Berkeley National Laboratory. This setup consists of a commercial nanoscope (neaspec neaSNOM) coupled to a Cu:Ge detector and a silicon beamsplitter.[37] Amplitude and phase were collected over the frequency range of 330-700 cm^{-1} and with a tip-limited spatial resolution on the order of 20 x 20 nm^2. All near-field spectra employ second harmonic signals. For comparison, we measured traditional infrared absorption and Raman scattering using a Bruker 113v spectrometer equipped with a bolometer (20 - 700 cm^{-1}, 2 cm^{-1} resolution) and a Horiba LabRAM HR Evolution spectrometer (50 - 700 cm^{-1}, λ_{ex}= 532 nm at a power of 0.5 mW with an 1800 line/mm grating.) Ab-initio density functional theory (DFT) calculations were completed via Vienna ab-initio Simulation Package (VASP), which employs the projector-augmented wave (PAW) basis set.[38,39] For the treatment of electron correlations within DFT, a revised Perdew-Burke-Ernzerhof exchange-correlation functional for crystalline solids (PBEsol) was employed,[40] augmented by on-site Coulomb interactions for transition metal d-orbitals within a simplified rotationally-invariant form of the DFT+U_{eff} formalism.[41] Structural optimizations employed force criteria below 10^{-4} eV/Å. PHONOPY code interfaced with VASP was employed to calculate the Γ-point phonon mode frequencies for each structure.[42]

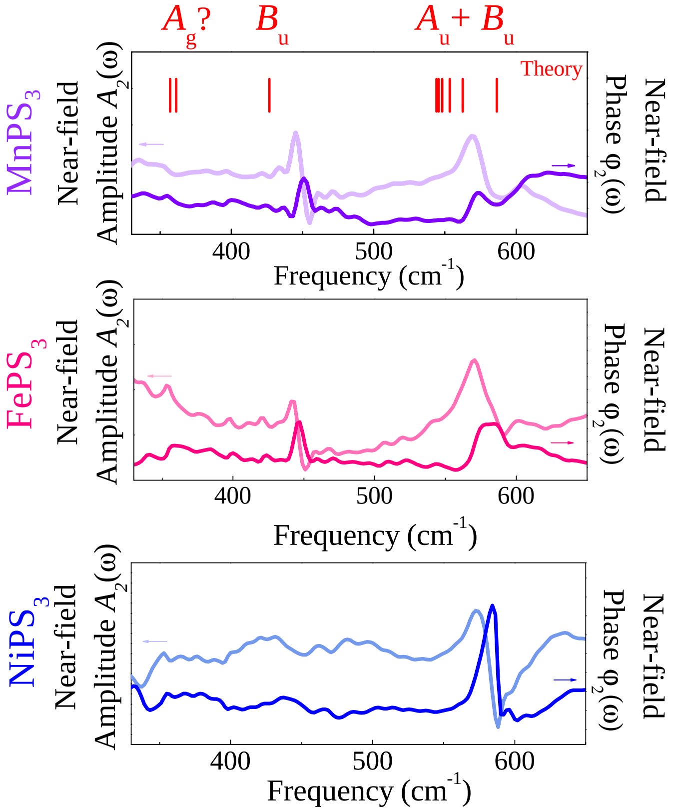

FIG. 2: Near-field amplitude and phase spectra for $MnPS_3$, $FePS_3$, and $NiPS_3$ single crystals at room temperature. Calculated mode positions and assignments are shown in the upper panel. The overall scale focuses on the currently available near-field frequency window (330 - 650 cm^{-1}) of interest.

Results and Discussion

Figure 2 summarizes the near-field spectra for the full set of MPS_3 materials (M = Mn, Fe, Ni). Both amplitude and phase signals are included to illustrate how this method works on single crystals and, at the same time,

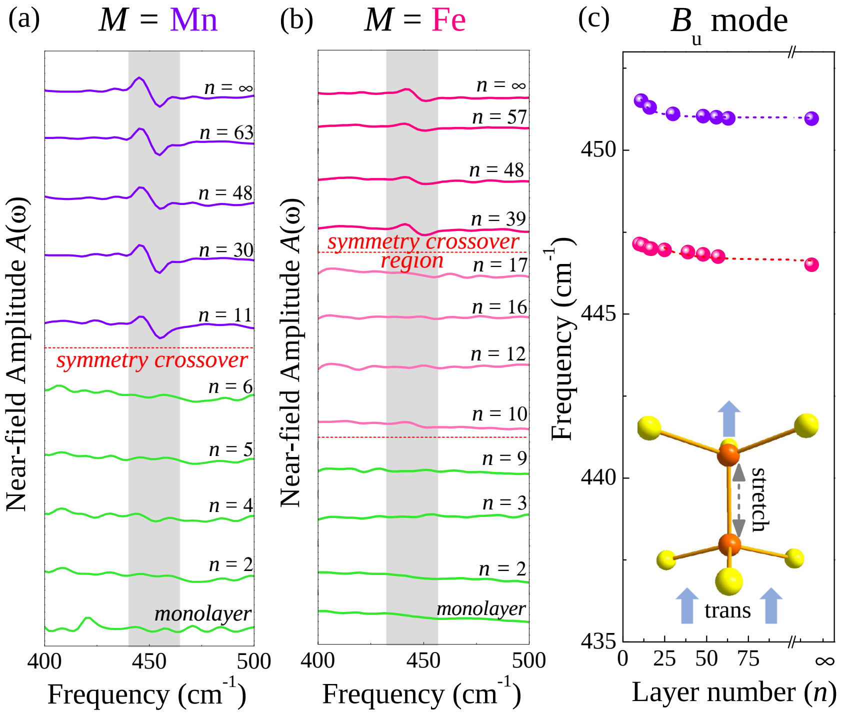

FIG. 3: (a, b) Close-up view of the near- field infrared response highlighting the behavior of the B_u symmetry vibrational mode in the M = Mn and Fe materials. Below $n = 11$ (Mn) and $n = 10$ (Fe), the data is multiplied by a factor of 5. The symmetry crossover is indicated, below which the B_u symmetry feature disappears. (c) Frequency vs. layer number trends for the M = Mn and Fe compounds showing how the B_u symmetry mode hardens on approach to the symmetry crossover. The dotted lines are a 1/size^2 fit to the data points. Error bars are smaller than the symbol size. A schematic view of the displacement pattern of the B_u mode is also included. The motion is a P–P stretch combined with in-phase, out-of-plane PS_3 translation.

to provide the $n = \infty$ response. Here, n is the layer number. Vibrational mode assignments are made via comparison with traditional infrared and Raman scattering spectra (Supplemental Information[43]) as well as prior lattice dynamics calculations of $MnPS_3$.[34] The high frequency doublet structure, centered near 567 cm^{-1} (Mn), 580 cm^{-1} (Fe), and 584 cm^{-1} (Ni), is clearly representative of the traditional infrared active A_u + B_u modes, with an isotope-like effect evident in the frequency progression. The B_u mode near 450 cm^{-1} is also present in the near-field spectrum of the Mn and Fe materials and significantly amplified compared to the far field infrared response. This feature is absent in $NiPS_3$. The 365 cm^{-1} feature in $MnPS_3$ is tentatively assigned as an A_g symmetry mode, activated by the tip-enhanced nature of the near-field technique.[34] A similar structure is observed near 357 cm^{-1} in $FePS_3$. A complete set of mode assignments and a brief discussion of signal-to-noise considerations is available in Supplemental Information.[43]

Figure 3 displays a close-up view of the near-field infrared response of $MnPS_3$ and $FePS_3$, focusing on the behavior of the B_u vibrational mode. The displacement pattern of this odd-symmetry (*ungerade*) mode is a P–P stretch combined with in-phase, out-of-plane PS_3 translation. This feature is very prominent in the spectrum of the $MnPS_3$ and $FePS_3$ single crystals. It is strong and well-resolved in few-layer $MnPS_3$ as well, shifting to higher frequency with decreasing layer number, consistent with expectations for confinement. Importantly, the B_u mode disappears below $n = 11$, indicative of a symmetry crossover in which the C_3 rotation is restored.[34] In other words, the $C2/m$ space group characterizes the $MnPS_3$ single crystal as well as the few-layer system down to approximately $n = 11$. At smaller n, the signature of the B_u mode is lost - evidence for a transition to a higher symmetry state [Fig. 3(a)]. A correlation group analysis and first principles modeling of the pattern of excitations reveals that the higher symmetry space group at small n and in the monolayer is $P\bar{3}1m$. Temperature effects may be partially responsible for the restoration of the C_3 rotation, although as we discuss below, crossovers between $C2/m$ and $P\bar{3}1m$ are seen in other contexts.

Because the B_u mode is such a sensitive indicator of symmetry, we extended this analysis to other members of the MPS_3 family with the goal of developing structure-property relationships. As shown in Fig. 3(b), the behavior of the B_u mode in $FePS_3$ is different than that in the Mn analog. As before, the B_u mode is strong and well-defined in the large n regime. This system reveals a gradual crossover to the high symmetry state. For instance, the B_u feature seemingly disappears after $n =$ 17, only to reappear below $n = 12$. Thus, the symmetry crossover seems to take place across a region rather than at a specific layer number, as is the case for $MnPS_3$. However, we still find the same $C2/m \rightarrow P\bar{3}1m$ symmetry increase on approach to the monolayer. Figure 3(c) shows frequency vs. layer number trends for the B_u mode. We find overall blue shifts on the order of 1 - 1.5 cm^{-1}. Although at the limit of our sensitivity, the Mn system appears to be fairly rigid until the symmetry crossover is approached whereas the Fe analog shifts systematically with decreasing layer number [Fig. 3(d)]. Fits to 1/size^2 are indicative of traditional quantum confinement, and the larger prefactor in $MnPS_3$ is consistent with enhanced sensitivity to strain.

Figure 4 summarizes the near-field infrared response

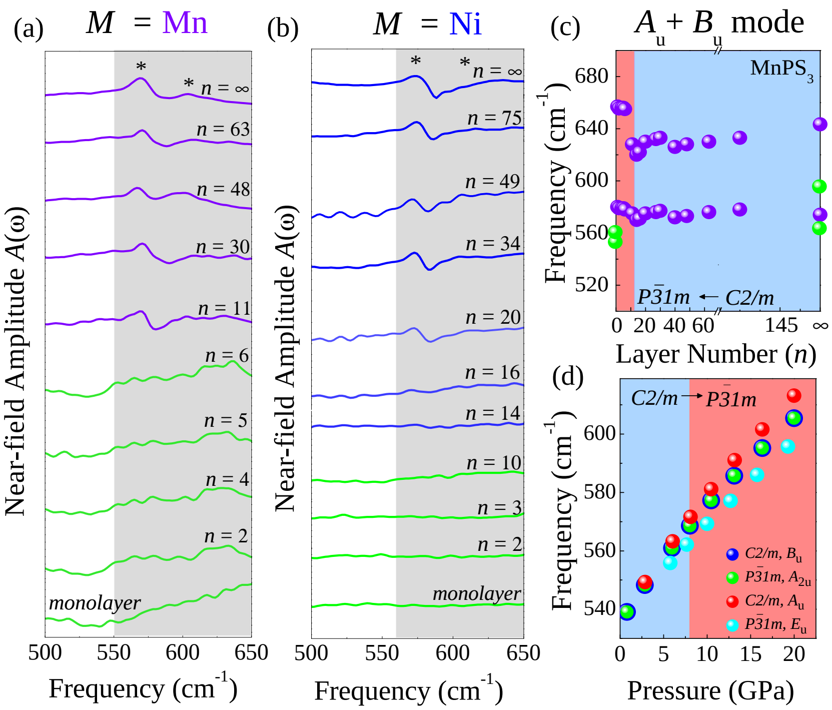

FIG. 4: Close-up view of the near-field infrared response in the region of the $A_u + B_u$ modes for the (a) Mn and (b) Ni materials at 300 K. The symmetry crossover is indicated by the change of color (blue ↔ green). (c) Frequency vs. layer number trend for MnPS$_3$ across the $C2/m \rightarrow P\bar{3}1m$ transition for both experiment (violet) and theory (green). Error bars are smaller than the symbol size. (d) Theoretically predicted frequency shift of MnPS$_3$ across the pressure-induced $C2/m \rightarrow P\bar{3}1m$ sliding transition.

of the $A_u + B_u$ sulfur-phosphorous stretching modes for this family of MPS$_3$ compounds (M = Mn, Fe, Ni) as a function of layer number. In each case, the $n = \infty$ spectra evolves with decreasing thickness - always sporting a clear doublet pattern in this frequency regime. The doublet structure is denoted by asterisks [Fig. 4]. In MnPS$_3$, the low frequency branch of the doublet red shifts with decreasing thickness whereas the high frequency branch blue shifts slightly. There is significant broadening between $n = 28$ and 22. Between $n = 16$ and 11, the two branches come together slightly and begin to diminish. This change in spectral features is attributed to the symmetry crossover.[34] Below $n = 11$, the features broaden dramatically and upshift slightly as the monolayer is approached. Eventually (when $n = 1$), the doublet structure that is the signature of the $A_u + B_u$ modes is overcome by the gold$\cdots$sulfur charge transfer band[44] above 550 cm^{-1} and cannot be resolved. Our lattice dynamics calculations reveal that there are a number of sulfur-phosphorous-related stretching modes that underlie the strong doublet pattern in this frequency region.[34] Plotting peak position vs. layer number, we see that both structures soften with decreasing n in the $C2/m$ phase, consistent with the notion that reducing inter-layer interactions tends to soften a resonance [Fig. 4(d)]. We find, however, that both features show a marked upturn across the $C2/m \rightarrow P\bar{3}1m$ transition.

The strong doublet structure that is characteristic of the $A_u + B_u$ sulfur-phosphorous stretching modes is clearly recognizable in NiPS$_3$ as well. It remains quite strong until $n = 16$, below which it becomes much less intense and then starts to broaden below $n = 14$. This doublet structure is, however, clearly retained at small n, suggesting that no symmetry crossover occurs in this material. The significantly smaller van der Waals gap and sheet thickness is anticipated to make NiPS$_3$ less vulnerable to temperature and strain effects than the Mn and Fe analogs. Interestingly, the charge transfer band,[44] present in the Mn (and Fe analogs) is absent in the near-field infrared spectrum of the NiPS$_3$ monolayer.

Bringing these trends together, we find that monoclinicity in the MPS$_3$ family of materials is the result of long-range stacking, temperature effects, and local structure. In other words, inter-slab proximity and thermally-induced structural fluctuations work to restore the C_3 rotation in small n members of the MPS$_3$ series for M = Mn and Fe.[45] Thus $P\bar{3}1m$ symmetry prevails in few-layer sheets of MnPS$_3$ and FePS$_3$ as well as the monolayers. Interestingly, the n dependence of the $C2/m$ to $P\bar{3}1m$ symmetry crossover is not related to slab thickness or van der Waals gap in a straightforward manner.

On the other hand, if we consider thicker two-dimensional layers and larger van der Waals gaps to be associated with changes in chemical bonding and weaker inter-slab proximity effects, we can develop some loose structure-property relationships. For instance, the van der Waals gap in NiPS$_3$ is the smallest of the series [Fig. 1(a)], so we expect inter-layer interactions to be the strongest. Proximity effects from adjacent layers may therefore constrain the Ni compound to the high symmetry $P\bar{3}1m$ state over the full n range. This supposition is consistent with the total absence of the B_u symmetry vibrational mode in the near-field infrared response of NiPS$_3$. This higher order space group is in contrast to prior x-ray diffraction work,[46–48] although because $C2/m$ is a subgroup of $P\bar{3}1m$, they can have nearly indistinguishable diffraction patterns. Moreover, the van der Waals gap in $MnPS_3$ and $FePS_3$ is significantly larger, which may provide additional flexibility as well as greater sensitivity to temperature. This picture is consistent with the discovery of pressure-induced sliding in $FePS_3$,[20] which also benefits from a larger van der Waals distance and weaker inter-layer interactions.

At the same time, the MPS$_3$ series has well-known trends in sheet thickness [Fig. 1(a)]. The Mn and Fe compounds are nearly the same macroscopically (as indicated by their sheet thicknesses and van der Waals gaps) but not microscopically (in terms of their bond lengths and angles), whereas $NiPS_3$ has an overall contraction of the lattice compared to the other two systems. Trends in the P–P bond length are straightforward and follow the sheet thickness trend - decreasing across the family from Mn to Ni. The 4% drop in the Ni compound creates a "pinch point", which leads to additional sheet corrugation. The P–S bonds also decrease systematically across the series by about 3.5%, although the difference is largest between the Mn and Fe analogs. In general, the M–S bonds also get shorter in the Mn to Ni series. The overall difference is on the order of 3%, although there are slight variations. $NiPS_3$ is a special case. Here, the M–S distances are nearly identical. This is consistent with a high symmetry state (especially compared to kT) and suggests that $NiPS_3$ might be $P\bar{3}1m$ (or very close to $P\bar{3}1m$) all along rather than $C2/m$ as suggested by x-ray diffraction work.[46–48] That the C_3 symmetry element is located at the metal center is in line with this supposition. This finding is also consistent with the lack of a B_u mode signature in the bulk single crystal [Fig. 2(c)] or in any of the sheets. That bond distances are overall longer in $MnPS_3$ compared to $NiPS_3$ consistent with greater ionic (and less covalent) character to the bonds.

Angular trends also impact the symmetry in the MPS$_3$ family of materials. Overall, the S–P–S angles are very similar, and the differences between these angles get smaller as we go across the Mn to Fe to Ni series. This is consistent with more "C_3-ness" and higher order symmetry. Such a trend would, again, tend to suppress the B_u vibrational mode. The S–M–S angle is different. It increases across the $MnPS_3$ to $NiPS_3$ series, and because changes in this angle move the metal center inward, the overall effect is to increase corrugation. Not only do differences in the S–M–S angle increase across the series, but this angle also differentiates $MnPS_3$ from $FePS_3$. Angular effects may also explain why $NiPS_3$ is unable to stabilize a magnetic ground state in monolayer form.[13] A full table of bond lengths and angles is provided in the Supplemental Information.[16,17,43]

Finally, we point out that the space groups preferred by $MnPS_3$ under confinement are strikingly similar to those under compression. Pressure-induced sliding in $MnPS_3$ and the Fe analog involves a $C2/m \to P\bar{3}1m$ transition.[20,23] Evidence for this crossover is subtle in the phonon response and consists of a slight frequency shift across the critical pressure.[23] The $A_u + B_u$ modes of $MnPS_3$, for instance, are predicted to show a slope change across the $C2/m \to P\bar{3}1m$ sliding transition [Fig. 4(e)]. This comparison was carried out by performing both energy and lattice dynamics calculations in the two different phases.[23] Exfoliated $MnPS_3$ shows a clear frequency shift across the $C2/m \to P\bar{3}1m$ transition at n = 11 as well, although the frequencies harden (rather than soften) in few-sheet form [Fig. 4(d)]. The fact that exerting pressure and reducing layer thickness show opposite tendencies is perfectly understandable. The former enhances three-dimensionality, whereas the latter does the opposite. It is more challenging to understand why exerting pressure softens rather than hardens the phonon modes. We speculate that external pressure suppresses the band gap,[23] and the enhanced charge fluctuations can be expected to better screen electrostatic potentials thus softening the phonon modes. Making the sample thinner should reduce layer-normal band dispersion, contributing to larger band gap, reduced charge excitations and screening, with resulting harder phonon modes. Interestingly, the symmetry of $MnPS_3$ is also predicted to switch back to $C2/m$ across the pressure-driven insulator-metal transition.[23] These commonalities indicate that the C_3 rotation is a rather fragile symmetry element in the $MnPS_3$ system, which is indeed the case due to its partially-filled t_{2g} configuration in proximity to its pressure-induced low-spin metallic configuration.[23] On the other hand, the fully occupied t_{2g} shell in $NiPS_3$ is consistent with its C_3-symmetric structure as proposed in this work.[49]

Conclusion

To summarize, we employed synchrotron-based near-field infrared nano-spectroscopy to explore the symmetry crossover in the MPS$_3$ (M = Mn, Fe, Ni) family of materials in bulk, few-, and single-layer form as well as the structure-property relations that can be unraveled in these systems. In $MnPS_3$, the B_u symmetry mode near 450 cm^{-1} - which probes the P–P stretch combined with in-phase, out-of-plane PS_3 translation - is exquisitely sensitive to the $C2/m \to P\bar{3}1m$ transition that takes place at layer number 11. A similar effect occurs in $FePS_3$. The complete loss of the B_u mode in both materials demonstrates that symmetry is increased the thinnest sheets. There are also a few subtle differences. In $FePS_3$, the $C2/m \to P\bar{3}1m$ crossover takes place over a range of thicknesses (rather than at $n = 11$ as in the Mn compound), and it responds gradually to strain as evidenced by the systematic frequency shift with decreasing layer number (different from $MnPS_3$, which is fairly rigid as the crossover is approached). Strikingly, the third member of this family of materials, $NiPS_3$, does not show a symmetry crossover with decreasing sheet thickness. This is because $NiPS_3$ already exists as $P\bar{3}1m$ (or very close to $P\bar{3}1m$) in bulk form - at least at room temperature - due to the lack of a clear B_u symmetry vibrational mode in the spectroscopic response. We analyze these effects in terms of the stronger interlayer interactions present in the Ni system as well as the local structure within the layer itself. Taken together, we find that monoclinicity in this family of materials is a consequence of long range stacking, temperature effects, and local lattice distortions.

Acknowledgments

Research at the University of Tennessee is supported by the U.S. Department of Energy, Office of Basic Energy Sciences, Materials Science Division under award DE-FG02-01ER45885 (J.L.M.). Work at Rutgers University is funded by the National Science Foundation DMREF program (DMR-1629059). D.G.M. acknowledges support from the Gordon and Betty Moore Foundation's EPiQS Initiative through Grant GBMF9069. A.V.H. acknowledges funding from the Center for Materials Processing, a Tennessee Higher Education Commission (THEC) supported Accomplished Center of Excellence, for funding the crystal synthesis work that provided materials for this research. Portions of these measurements utilized beamline 2.4 at the Advanced Light Source, which is a DOE Office of Science User Facility operated under contract no. DE-AC02-05CH11231, including the remote user program from NSLS-II under contract DE-SC0012704.

References

[*] Electronic address: `musfeldt@utk.edu`

[1] L. D. Casto, A. J. Clune, M. O. Yokosuk, J. L. Musfeldt, T. J. Williams, H. L. Zhuang, M. W. Lin, K. Xiao, R. G. Hennig, B. C. Sales, J. Q. Yan, and D. Mandrus. APL Materials **3**, 041515 (2015).

[2] H. Yang, S. W. Kim, M. Chhowalla, and Y. H. Lee. Nature Physics **13**, 931 (2017).

[3] S. Li, Z. Ye, X. Luo, G. Ye, H. H. Kim, B. Yang, S. Tian, C. Li, H. Lei, A. W. Tsen, K. Sun, R. He, and L. Zhao. Physical Review X **10**, 011075 (2020).

[4] I. Lee, F. G. Utermohlen, D. Weber, K. Hwang, C. Zhang, J. Van Tol, J. E. Goldberger, N. Trivedi, and P. C. Hammel. Physical Review Letters **124**, 017201 (2020).

[5] A. B. Kaul. Journal of Materials Research **29**, 348 (2014).

[6] X. Zhang, X.-F. Qiao, W. Shi, J.-B. Wu, D.-S. Jiang, and P.-H. Tan. Chemical Society Reviews **44**, 2757 (2015).

[7] C. T. Kuo, M. Neumann, K. Balamurugan, H. J. Park, S. Kang, H. W. Shiu, J. H. Kang, B. H. Hong, M. Han, T. W. Noh, and J. G. Park. Scientific Reports **6**, 1 (2016).

[8] J.-U. Lee, S. Lee, J. H. Ryoo, S. Kang, T. Y. Kim, P. Kim, C.-H. Park, J.-g. Park, and H. Cheong. Nano Letters **16**, 7433 (2016).

[9] B. Huang, G. Clark, E. Navarro-Moratalla, D. R. Klein, R. Cheng, K. L. Seyler, D. Zhong, E. Schmidgall, M. A. McGuire, D. H. Cobden, W. Yao, D. Xiao, P. Jarillo-Herrero, and X. Xu. Nature **546**, 270 (2017).

[10] G. Long, T. Zhang, X. Cai, J. Hu, C. W. Cho, S. Xu, J. Shen, Z. Wu, T. Han, J. Lin, J. Wang, Y. Cai, R. Lortz, Z. Mao, and N. Wang. ACS Nano **11**, 11330 (2017).

[11] L. Zhong, X. Chen, and J. Qi. Physical Chemistry Chemical Physics **19**, 15388 (2017).

[12] Y.-J. Sun, Q.-H. Tan, X.-L. Liu, Y.-F. Gao, and J. Zhang. The Journal of Physical Chemistry Letters **10**, 3087 (2019).

[13] K. Kim, S. Y. Lim, J. U. Lee, S. Lee, T. Y. Kim, K. Park, G. S. Jeon, C. H. Park, J. G. Park, and H. Cheong. Nature Communications **10**, 1 (2019).

[14] P. A. Joy and S. Vasudevan. Journal of Physics and Chemistry of Solids **54**, 343 (1993).

[15] Y. Mathey, R. Clement, C. Sourisseau, and G. Lucazeau. Inorganic Chemistry **19**, 2773 (1980).

[16] G. Ouvrard, R. Brec, and J. Rouxel. Materials Research Bulletin **20**, 1181 (1985).

[17] W. Klingen, E. G., and H. Hanh. Journal of Inorganic and General Chemistry **401**, 97 (1973).

[18] K. Z. Du, X. Z. Wang, Y. Liu, P. Hu, M. I. B. Utama, C. K. Gan, Q. Xiong, and C. Kloc. ACS Nano **10**, 1738 (2016).

[19] N. Sivadas, S. Okamoto, and D. Xiao. Physical Review Letters **117**, 267203 (2016).

[20] C. R. Haines, M. J. Coak, A. R. Wildes, G. I. Lampronti, C. Liu, P. Nahai-Williamson, H. Hamidov, D. Daisenberger, and S. S. Saxena. Physical Review Letters **121**, 266801 (2018).

[21] F. Wang, T. A. Shifa, P. Yu, P. He, Y. Liu, F. Wang, Z. Wang, X. Zhan, X. Lou, F. Xia, and J. He. Advanced Functional Materials **28**, 1 (2018).

[22] C. M. Pasco, I. El Baggari, E. Bianco, L. F. Kourkoutis, and T. M. McQueen. ACS Nano **13**, 9457 (2019).

[23] N. Harms, H.-S. Kim, A. J. Clune, K. Smith, K. R. O'Neal, A. Haglund, D. G. Mandrus, Z. Liu, K. Haule, D. Vanderbilt, and J. L. Musfeldt. Nature Quantum Materials Under review. (2020).

[24] K. Kyriazi and J. Singleton In preparation.

[25] H. Li, Q. Zhang, C. C. R. Yap, B. K. Tay, T. H. T. Edwin, A. Olivier, and D. Baillargeat. Advanced Functional Materials **22**, 1385 (2012).

[26] J. Lee, T. Y. Ko, J. H. Kim, H. Bark, B. Kang, S. G. Jung, T. Park, Z. Lee, S. Ryu, and C. Lee. ACS Nano **11**, 10935 (2017).

[27] H. A. Bechtel, E. A. Muller, R. L. Olmon, M. C. Martin, and M. B. Raschke. Proceedings of the National Academy of Sciences **111**, 7191 (2014).

[28] E. A. Muller, B. Pollard, and M. B. Raschke. Journal of Physical Chemistry Letters **6**, 1275 (2015).

[29] M. Hafeez, L. Gan, H. Li, Y. Ma, and T. Zhai. Advanced Functional Materials **26**, 4551 (2016).

[30] A. Alkabsh, H. Samassekou, and D. Mazumdar. Nanotechnology **30**, 1 (2019).

[31] M. Patel, J. Kim, and Y. K. Kim. Advanced Functional Materials **28**, 1 (2018).

[32] Y. R. Sapkota and D. Mazumdar. Journal of Applied Physics **124**, 105306 (2018).

[33] J. Chen, M. Badioli, P. Alonso-González, S. Thongrattanasiri, F. Huth, J. Osmond, M. Spasenović, A. Centeno, A. Pesquera, P. Godignon, A. Zurutuza Elorza, N. Camara, F. J. G. de Abajo, R. Hillenbrand, and F. H. L. Koppens. Nature **487**, 77 (2012).

[34] S. N. Neal, H.-S. Kim, K. A. Smith, A. V. Haglund, D. G. Mandrus, H. A. Bechtel, G. L. Carr, K. Haule, D. Vanderbilt, and J. L. Musfeldt. Physical Review B **100**, 075428 (2019).

[35] K. A. Smith, E. A. Nowadnick, S. Fan, O. Khatib, S. J.

Lim, B. Gao, N. C. Harms, S. N. Neal, J. K. Kirkland, M. C. Martin, C. J. Won, M. B. Raschke, S. W. Cheong, C. J. Fennie, G. L. Carr, H. A. Bechtel, and J. L. Musfeldt. Nature Communications **10**, 1 (2019).

[36] R. Nitsche and P. Wild. Materials Research Bulletin **5**, 419 (1970).

[37] O. Khatib, H. A. Bechtel, M. C. Martin, M. B. Raschke, and G. L. Carr. ACS Photonics **5**, 2773 (2018).

[38] G. Kresse and J. Furthmüller. Physical Review B **54**, 11169 (1996).

[39] G. Kresse and D. Joubert. Physical Review B **59**, 1758 (1999).

[40] J. P. Perdew, A. Ruzsinszky, G. I. Csonka, O. A. Vydrov, G. E. Scuseria, L. A. Constantin, X. Zhou, and K. Burke. Physical Review Letters **100**, 136406 (2008).

[41] S. L. Dudarev, G. A. Botton, S. Y. Savrasov, C. J. Humphreys, and A. P. Sutton. Physical Review B **57**, 1505 (1998).

[42] A. Togo and I. Tanaka. Scripta Materialia **108**, 1 (2015).

[43] See Supplemental Information at [XXX] for traditional infrared and Raman spectra, tables with displacement patterns and bond lengths/angles, and a discussion on signal-to-noise ratio in the near-field infrared response of atomically thin materials.

[44] E. Pensa, E. Cortés, G. Corthey, P. Carro, C. Vericat, M. H. Fonticelli, G. Benítez, A. A. Rubert, and R. C. Salvarezza. Accounts of Chemical Research **45**, 1183 (2012).

[45] These thermal fluctuations are not an effect of the incident light but rather of room temperature.

[46] N. Ismail, Y. M. Temerk, A. A. El-Meligi, M. A. Badr, and M. Madian. Journal of Solid State Chemistry **183**, 984 (2010).

[47] R. N. Jenjeti, R. Kumar, M. P. Austeria, and S. Sampath. Scientific Reports **8**, 1 (2018).

[48] Z. Ur Rehman, Z. Muhammad, O. A. Moses, W. Zhu, C. Wu, Q. He, M. Habib, and L. Song. Micromachines **9**, 1 (2018).

[49] Unlike in the corner-shared geometries such as perovskite structures, partially filled e_g configurations very weakly couple to the lattice and show almost no Jahn-Teller instability.